Journal of Medicinal Chemistry

pubs.acs.org/jmc

Article

Development and Nanoparticle-Mediated Delivery of Novel MDM2/MDM4 Heterodimer Peptide Inhibitors to Enhance 5-Fluorouracil Nucleolar Stress in Colorectal Cancer Cells

Francesco Merlino,[§] Annalisa Pecoraro,[§] Giuseppe Longobardi, Greta Donati, Francesco Saverio Di Leva, Chiara Brignola, Rebecca Piccarducci, Simona Daniele, Claudia Martini, Luciana Marinelli, Giulia Russo, Fabiana Quaglia, Claudia Conte,* Annapina Russo,* and Valeria La Pietra*

Cite This: *J. Med. Chem.* 2024, 67, 1812−1824

Read Online

ACCESS | Metrics & More | Article Recommendations | Supporting Information

ABSTRACT: Colorectal cancer (CRC) often involves wild-type p53 inactivation by MDM2 and MDM4 overexpression, promoting tumor progression and resistance to 5-fluoruracil (5-FU). Disrupting the MDM2/4 heterodimer can proficiently reactivate p53, sensitizing cancer cells to 5-FU. Herein, we developed 16 peptides based on Pep3 (**1**), the only known peptide acting through this mechanism. The new peptides, notably **3** and **9**, showed lower IC_{50} values than **1**. When incorporated into tumor-targeted biodegradable nanoparticles, these exhibited cytotoxicity against three different CRC cell lines. Notably, NPs/**9** caused a significant increase in p53 levels associated with a strong increment of its main downstream target p21 inducing apoptosis. Also, the combined treatment of **9** with 5-FU caused the activation of nucleolar stress and a synergic apoptotic effect. Hence, the co-delivery of MDM2/4 heterodimer disruptors with 5-FU through nanoparticles might be a promising strategy to overcome drug resistance in CRC.

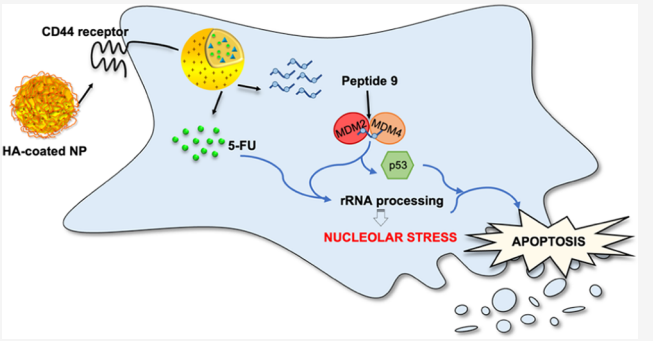

INTRODUCTION

According to the Global Cancer Observatory, colorectal cancer (CRC) is one of the most common types of tumor worldwide. In 2020, nearly 2 million new cases have been reported and despite significant breakthroughs in the understanding, prevention, and treatment of CRC, it still accounts for 9.4% (935,173) of cancer-related deaths.[1] Today, the standard care for CRC depends on the tumor's specific stratification and staging. Generally, patients with stages I−III CRC undergo surgical resection when possible, followed by adjuvant therapy, which typically includes the cytotoxic agent 5-fluorouracil (5-FU) alone or in combination with oxaliplatin (FOLFOX) or irinotecan (FOLFIRI).[2]

5-FU inhibits the thymidylate synthase (TS), an enzyme involved in nucleotide synthesis necessary for cell growth, thus impairing both rDNA and rRNA syntheses, driving alterations of nucleolar structure and function, and compromising many fundamental cellular processes.[3] In addition, metabolites of 5-FU also act as rRNA intercalators, leading to the disruption of rRNA processing, which, in turn, activates a complex cellular response, namely, nucleolar stress. The nucleolar stress response integrates several pathways, some of which involve the tumor suppressor p53.[4]

p53 is a transcription factor that regulates the expression of more than a hundred target genes involved in essential cellular processes, such as cell cycle progression, DNA repair, apoptosis, autophagy, senescence, and differentiation.[5] In physiological conditions, p53 activity is finely controlled by MDM2 (murine double minute 2), namely, the ubiquitin E3 ligase that negatively regulates p53, promoting its degradation *via* ubiquitination,[5] and its analogue MDM4 (murine double minute 4), which binds p53 and inhibits its transactivation.[6,7] In the absence of stress signals, MDM2 restricts the growth-suppressive function of p53, maintaining low cellular levels of this protein, and MDM4 guarantees a nuclear pool of transcriptionally incompetent p53.[6] During the p53-dependent nucleolar stress response, several nucleolar and/or ribosomal proteins from the large and small subunits translocate to the nucleoplasm and bind to MDM2,

Received: July 20, 2023
Revised: December 29, 2023
Accepted: January 9, 2024
Published: January 29, 2024

https://doi.org/10.1021/acs.jmedchem.3c01312
J. Med. Chem. 2024, 67, 1812−1824

resulting in p53 stabilization and consequent induction of p53-mediated cell cycle arrest or apoptosis.[8]

Alterations in the p53 pathway can significantly affect the sensitivity to cytotoxic CRC chemotherapy.[9] In fact, CRC, along with other malignancies, evades cell death and develops drug resistance by maintaining low levels of p53 through the hyperactivation of MDM2 and/or MDM4.[9,10] In this regard, it has already been demonstrated that inhibiting the interaction between p53 and both MDMs (by double MDM2/4 knockdown or using dual inhibitors) can sensitize CRC cells to well-known chemotherapeutic agents, including 5-FU.[11]

In this context, many efforts have been carried out in the last few decades to develop very potent MDM2 inhibitors, with some of them in clinical trials.[12] Although these molecules cause p53 reactivation, a modest p53-dependent apoptotic response is frequently observed in cancer cells due to their lack of activity on MDM4.[13] While numerous groups were hence struggling to develop molecules are able to simultaneously dissociate p53 from both MDM2 and MDM4, genetic evidence suggested that an efficient inhibition of p53 is obtained by the formation of MDM2/MDM4 heterodimers,[14] opening the road to a novel approach for cancer therapy. In fact, it is well-known that although MDM2 and MDM4 share a high level of similarity, only MDM2 can ubiquitinate and, in turn, degrade p53. On the other hand, MDM4 is absolutely important for the effective degradation of p53, as it is able to stimulate and enhance the MDM2 activity by the formation of the MDM2/MDM4 heterodimer.[15] Also, the MDM2/MDM4 heterodimer has been found at the target gene promoters inhibiting p53 transcription activity.[16] The fact that the heterodimer is necessary for proper control of p53 activity is supported by genetic experiments. Indeed, it has been shown that mice-expressing MDM4 mutants defecting in MDM2 binding die during embryonic development.[14,17] Consequently, the MDM2 and MDM4 interface became an attractive target for proficient p53 reactivation and to achieve oncosuppressive function. In this light, there is evidence that the combination of 5-FU with MDM2/4 heterodimer disruptors can represent a useful therapeutic strategy to improve the efficacy of adjuvant chemotherapy and overcome drug resistance in CRC. To date, only one molecule is known to inhibit the heterodimer formation, which is a dodecapeptide called Pep3 (**1**) (IC_{50} = 6.7 μM),[18] able to efficiently restore the p53 pathway and inhibit tumor growth. However, the low potency of **1** and its potential susceptibility to enzymatic degradation may represent great limitations. In fact, many therapeutic peptides suffer from poor physicochemical/biological stability that may limit their potential benefits and, in some cases, hamper their utility. Furthermore, when peptide therapeutics are developed for intracellular targets, their internalization and biological activity may be limited by inefficient membrane permeability and/or endosomal escape. The development of effective peptide delivery strategies is therefore essential to further enhance therapeutic outcomes to enable widespread medical applications.[19−21] In this context, nanotechnology has demonstrated great promise for peptide delivery.[22] Indeed, nanoparticle (NP) technologies can: (i) protect peptides from premature degradation or denaturation in the biological environment; (ii) enhance systemic circulation half-life of peptides with poor pharmacokinetic profiles; (iii) control sustained and/or tunable release, which can maintain drug concentration in the therapeutic range; and (iv) target diseased tissues, tumor cells, and intracellular compartments, thus improving the safety and efficacy of biological therapeutics.[23]

In particular, the employment of multifunctional polymeric NPs bearing different elements in a single entity offers an unprecedented tool for innovation. The employment of biocompatible and versatile polymers in NP design and the use of specific fabrication techniques can also allow the delivery of multiple drugs with different physicochemical properties in combinations, thus exerting a combined or even a synergic effect.[24]

Given these premises, the design, synthesis, NP delivery, and biological characterization of molecules able to disrupt the MDM2/4 heterodimer are herein reported. Starting from the structure of **1**, a library of shorter peptide analogues (consisting of 5−8 residues) has been developed. Intriguingly, the new peptides displayed lower IC_{50} values than **1** and, in particular, one of the most active peptides (herein named **9**, IC_{50} = 0.42 μM), loaded alone or together with 5-FU into poly(lactic-*co*-glycolic acid) (PLGA)-based NPs, proved to induce nucleolar stress, to restore apoptosis, and reduce CRC cell growth. Finally, molecular modeling studies disclosed the molecular basis of the binding of **9** at the MDM2/MDM4 interface, providing valuable clues for future drug design campaigns targeting this protein−protein interaction.

RESULTS AND DISCUSSION

It is known that the C-terminal RING finger domains of MDM2 and MDM4 interact with each other to form the MDM2/MDM4 heterodimer. Each RING domain possesses three central β-sheet motifs that form a tight β-barrel core at the interface. The structural characterization of the MDM2/MDM4 complex[25] showed that the interaction is mediated by the last C-terminal hydrophobic residues of the two proteins. In particular, with the aid of mutagenesis experiments, it was discovered that F490, L430, and A434, located at the C-terminus of MDM2, form a hydrophobic patch at the interface of the complex with residues L433 and I489 of MDM4. As hydrophobic patches play key roles in stabilizing protein−protein interactions,[26] this information has been used by Pellegrino et al. for the discovery of the peptide sequence Ac−^{479}KEIQLVIKVFIA^{490}-NH_2, named Pep3 (**1**).[18] This 12-mer peptide overlaps the C-terminus of MDM4 and has been shown to be able to reduce p53 ubiquitination, representing the only peptide inhibitor of the MDM2/4 complex known to date.

The analysis of the complex of **1** bound to MDM2 at the MDM4 interface (obtained by the MDM2/4 heterodimer complex PDB code: 2VJF)[25] led us to observe that while the peptide C-terminus is tightly bound to the hydrophobic hot spot of MDM2 formed by residues L430, A434, and F490 (Figure 1), the N-terminal region of **1** is found outside of this region. Precisely, it is in a solvent-exposed area, not interacting with any of the protein counterparts, and thus might not be crucial (even detrimental) for the interaction with the MDM2 RING domain.

Our design objective was to identify a truncated sequence derived from **1** by systematically deleting amino acids from the N-terminal end, with the expectation of achieving a higher binding affinity with MDM2. Additionally, to investigate the influence of charge variations on protein−peptide interactions, both N- (capped or not) and C-terminal (carboxylic acid or amide) modifications have been probed. Thus, a library of 16**1** derivatives, with sequence lengths ranging from 5- to 8-mer, was developed (Table 1).

https://doi.org/10.1021/acs.jmedchem.3c01312
J. Med. Chem. 2024, 67, 1812−1824

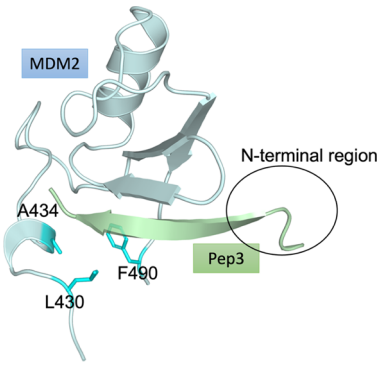

Figure 1. Complex structure of **1** (green ribbon) at the MDM4 interface of MDM2 (light blue ribbon; PDB code: 2VJF). In the black circle, the N-terminal region of **1**, which is far from the hydrophobic patch of MDM2, is shown.

Table 1. Name, Sequence, and IC_{50} Values of the Newly Synthesized MDM2/4 Heterodimer Peptide Disruptors

name	sequence	IC_{50} (μM)[b]
1[a]	Ac-KEIQLVIKVFIA-NH_2	6.7 ± 0.81
Acetylated N-Term, $-CO_2H$ as C-Term (Series A)		
2	Ac-LVIKVFIA−OH	4.35 ± 0.85
3	Ac-VIKVFIA−OH	0.64 ± 0.19
4	Ac-IKVFIA−OH	5.90 ± 0.70
5	Ac-KVFIA−OH	2.89 ± 0.93
Free N-Term, $-CONH_2$ as C-Term (Series B)		
6	H-LVIKVFIA-NH_2	2.90 ± 0.11
7	H-VIKVFIA-NH_2	3.76 ± 0.67
8	H-IKVFIA-NH_2	6.25 ± 0.65
9	H-KVFIA-NH_2	0.42 ± 0.01
Free N-Term, $-CO_2H$ as C-Term (Series C)		
10	H-LVIKVFIA−OH	n.a.
11	H-VIKVFIA−OH	3.77 ± 0.87
12	H-IKVFIA−OH	1.43 ± 0.28
13	H-KVFIA−OH	4.29 ± 0.82
Acetylated N-Term, $-CONH_2$ as C-Term (Series D)		
14	Ac-LVIKVFIA-NH_2	2.07 ± 0.57
15	Ac-VIKVFIA-NH_2	2.14 ± 0.50
16	Ac-IKVFIA-NH_2	2.75 ± 0.49
17	Ac-KVFIA-NH_2	7.25 ± 0.98

[a]**1** sequence.[13] [b]Results are the mean ± SEM of three independent measurements.

Chemistry. The synthesis of peptides **2**−**17** was performed by using the ultrasound-assisted solid-phase peptide synthesis (US-SPPS)[27] *via* the 9-fluorenylmethoxycarbonyl (Fmoc)/*tert*-butyl (*t*-Bu) orthogonal protection strategy. Briefly, the US-SPPS was employed for Fmoc-deprotection [20% piperidine in *N*,*N*-dimethylformamide (DMF), 0.5 + 1 min] and coupling [(1-cyano-2-ethoxy-2-oxoethylidenaminooxy)dimethylamino-morpholino-carbenium hexafluorophosphate (COMU)/Oxyma Pure as activating/additive agents, 5 min treatment] reactions, which were cyclically performed until the accomplishment of the resin-bound target linear peptide sequences. Upon cleavage from the solid support, crude peptides were purified by reversed-phase high-performance liquid chromatography (RP-HPLC). Each peptide was assessed for purity (>97%) by analytical RP-HPLC, and prior to biological investigations, the correct molecular mass was confirmed through high-resolution mass (HRMS) spectrometry (see the Supporting Information).

MDM2/4 Heterodimer Dissociation Assay. To test the ability of the synthesized compounds to disrupt the MDM2/4 complex, a dissociation assay was performed on lysates obtained from the MCF-7 tumor cells since they express a significantly high level of the MDM2/4 heterocomplex.[28] First, a calibration curve was performed, thus assessing the protein concentrations of MCF-7 cell lysates to be employed for our assay.[29] As reported in Figure S1, the absorbance (measured at 450 nm) proportionally increased with the concentration of the total proteins in MCF-7, showing a plateau starting from 25 μg of proteins in cell lysates. Therefore, the setup of the MDM2/4 dissociation assay was then performed and the ability, in terms of IC_{50}, of the tested compound to dissociate the complex was investigated through the homemade quantitative immunoenzymatic assay, using **1** as the reference compound (Table 1). Intriguingly, the newly truncated peptides displayed (with the only exception of **17**) IC_{50} values lower than **1**. Particularly, the most effective peptides were **3** and **9** with IC_{50} values of 0.64 and 0.42 μM, respectively. As shown in Figure S2, the inhibitory effect is dose-dependent.

Preparation and Characterization of NPs. These newly synthesized linear peptides degraded in the serum environment to a significant percentage within 1 h (~50%, Figure S3, see the Supporting Information), which can limit their possible administration. Consequently, an appropriate nanocarrier for their delivery has been developed, also in view of the poor ability of these compounds to overcome biological membranes and enter the cells. Biodegradable and polymeric NPs were prepared starting from PLGA and polyethylenimine (PEI). PLGA was selected for its well-known ability to load lipophilic drugs, whereas PEI was used to form a positively charged surface useful for the final coating. Furthermore, in the past few years, we have developed similar NPs that have demonstrated a great ability to load and deliver anticancer drugs into cancer cells, including CRC cells.[30,31] We conducted a preliminary formulation study to determine the optimal conditions for NP assembling. In particular, we found that the optimal ratio between PLGA and PEI was 20:1 w/w. NPs were prepared through nanoprecipitation: briefly, the polymers were codissolved in the presence of the active compounds, previously solubilized in EtOH, and then added to a water phase. After nanoprecipitation, the polymeric PLGA/PEI core was surrounded by a layer of hyaluronic acid (HA) in order to confer stealth properties to the system and to selectively reach the CRC cells through the binding of CD44 receptors,[30] overexpressed in different kinds of tumors, including HCT 116 cell line (Figure 2A).[31] The use of CRC-targeted NPs will expectantly confer a good safety profile to our molecules and to their combination with 5-FU with respect to the majority of classical MDM2 inhibitors, which showed hematological and gastrointestinal side effects in clinical trials.[12]

For an appropriate set of comparative materials, we prepared unloaded NPs, NPs loaded with only the peptides (NPs/**3** and NPs/**9**), NPs loaded with only 5-FU (NPs/5-FU), and finally combined NPs loaded with 5-FU in association with the peptides (NPs/5-FU/**3** and NPs/5-FU/**9**). All of the formulations were characterized in terms of size, PDI, ζ, and yield of the production process (Table 2).

The yield for the formulations was high (~70%), indicating that no extensive polymer/drug precipitation or NP aggregation occurred during preparation. All of the NPs showed a size around 120 nm and with low polydispersity indices and negative ζ-potential values, independently by the drug entrapped, thus

https://doi.org/10.1021/acs.jmedchem.3c01312
J. Med. Chem. 2024, 67, 1812−1824

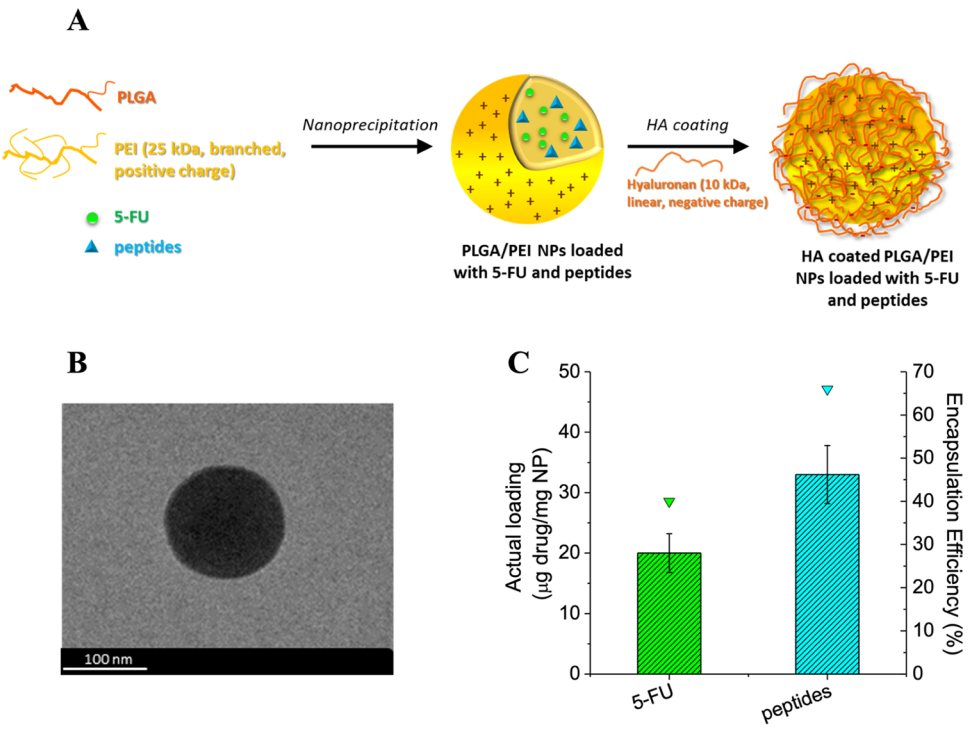

Figure 2. (A) Schematic illustration of NP structure and preparation through nanoprecipitation and HA layering procedure; (B) TEM image of NPs/5-FU/**9** as representative formulation; and (C) entrapment of 5-FU and peptides inside NPs. Results are the mean of three measurements obtained on three different NP batches ± SD.

Table 2. Composition and Properties of NPs

code	yield (%)	mean DH (nm ± SD[a])	PDI	ζ (mV ± SD[a])
unloaded NPs	75	112 ± 7	0.1	−29.9 ± 2.3
NPs/5-FU	70	114 ± 5	0.1	−29.8 ± 4.4
NPs/**3**	65	116 ± 9	0.2	−25.7 ± 2.7
NPs/**9**	72	119 ± 2	0.2	−21.2 ± 3.4
NPs/5-FU/**3**	70	115 ± 7	0.2	−23.9 ± 3.5
NPs/5-FU/**9**	75	117 ± 5	0.1	−20.9 ± 3.3

[a]SD was calculated on three different batches.

indicating the eventual propensity of this formulation to be intravenously injected. Concerning surface properties, the negative ζ-potential values are due to the presence of the outer shell of HA, electrostatically adsorbed on the cationic chains of PEI. These two polymers have also been quantified, and we found, in both cases, an adsorption of around 90% of the theoretical amount. The spherical morphology and the absence of NP aggregation were also confirmed by transmission electron microscopy (TEM) and scanning electron microscopy (SEM) images (Figures 2B and S4).

Concerning drug loading, NPs entrapped around 20 μg of 5-FU, in line with previous studies,[31] and 33 μg of peptides for mg of formulation, independently by the type of peptide and the encapsulation of one or two drugs together, thus indicating any interference between the compounds (Figure 2C). Then, to demonstrate the ability of NPs to deliver the drug cargo in a sustained manner, we have performed release studies in biological simulated conditions, and we have found that NPs released 5-FU as well as **9** along time. The reduction of the dose and the number of administrations are among the main advantages of using a nanocarrier for cancer treatment. In fact, the release of 5-FU is reported in Figure 3A, where it is clear that there is an initial burst release after around 6 h of incubation, corresponding to the release of 40% of the dose entrapped, and a second slower phase completed after 7 days. A similar trend was found for the release of **9** (Figure 3B).

Finally, to understand the behavior of NPs in the presence of proteins that can strongly modify the surface properties of a nanocarrier or induce aggregation/precipitation phenomena, we performed stability studies in the presence of fetal bovine serum (FBS), the main protein of the medium employed for cell studies. Indeed, the aggregation of proteins on the NP surface can modify its biological identity, thus influencing different NP properties, such as particle stability, biocompatibility, cellular uptake, and circulation lifetime.[32,33] To investigate this key issue, we incubated NPs in the presence of FBS and monitored the hydrodynamic diameter and turbidimetry of NP dispersions.

As clearly evidenced in Figure 3C, the size of NPs did not change in the presence of FBS up to 72 h of incubation, and no aggregation phenomena occurred (Figure 3D).

Cytotoxic Activity of NPs Loaded with Peptides. To demonstrate whether the investigated NPs could affect cell growth *in vitro*, we analyzed their cytotoxic activity against p53-proficient CRC cells. First, we verified the safety of the carrier: to this end, HCT 116 cells were incubated with unloaded NPs for 24, 48, and 72 h, and cell viability was tested by the 3-(4,5-dimethyl-thiazol-2-yl)-2,5-diphenyltetrazolium bromide (MTT) assay. As shown in Figure S5, no toxicity of unloaded NPs was found at 24 and 48 h, whereas a slight decrease in cell viability (~20%) was observed at 72 h. Then, HCT 116 cells were incubated with NPs/**3** and NPs/**9** at different concentrations for 24, 48, and 72 h, and cell viability was assessed by the MTT assay. As shown in Figure 4, the cytotoxic activity of both NPs was dose- and time-dependent. Nevertheless, HCT 116 cells displayed a different sensitivity to the two peptides loaded into NPs. In fact, growth inhibitory effects induced by NPs/**9** were higher than those observed for NPs/**3** at the same doses

https://doi.org/10.1021/acs.jmedchem.3c01312
J. Med. Chem. 2024, 67, 1812−1824

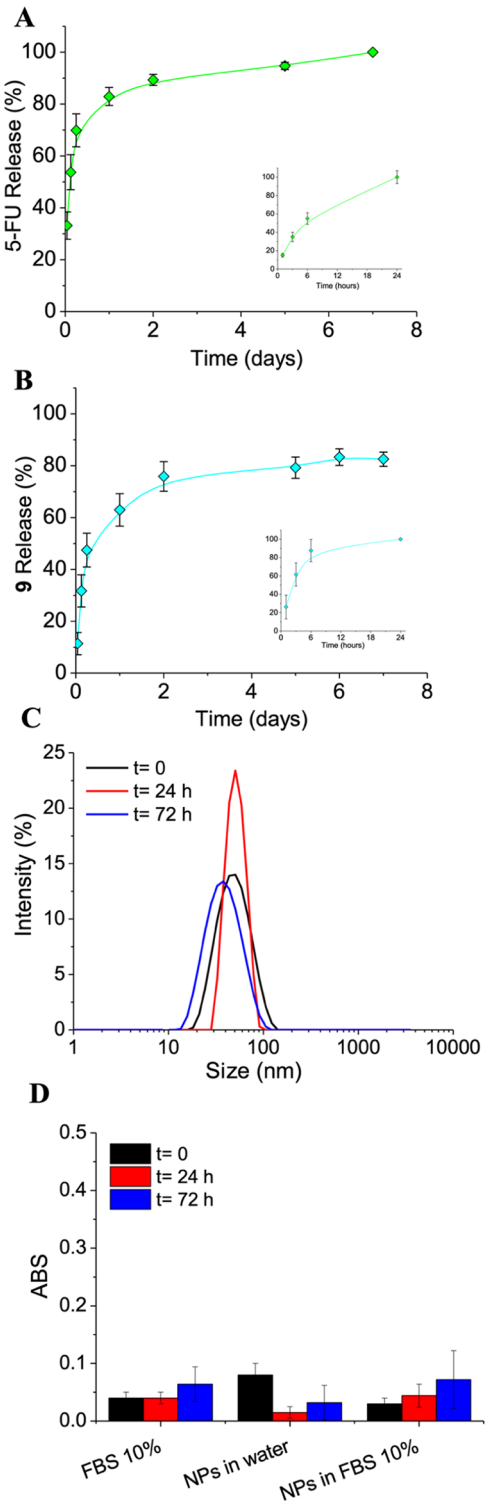

Figure 3. (A) Release studies of 5-FU from NPs. The release of free 5-FU is reported in the inset as control. (B) Release studies of **9** from NPs. The release of free **9** is reported in the inset as control. (C) Size distribution curves of NPs (0.5 mg/mL) in FBS at 10% at different time points. (D) Scattering of NPs incubated in FBS at 10% at different time points. Scattering of free FBS and NPs in water at the same concentration is reported as the control. Results are the mean of three measurements obtained on three different NP batches ± SD.

and time points. Specifically, NPs/**3** caused a reduction of cell viability of ∼40% after 72 h of treatment at the highest concentration tested (Figure 4A). In contrast, NPs/**9** treatment

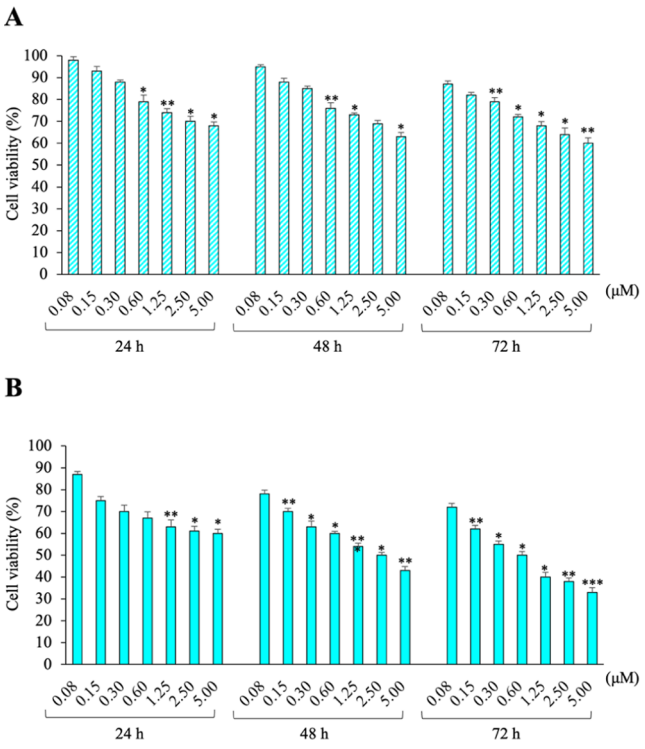

Figure 4. Cytotoxic effect of NPs/**3** (A) and NPs/**9** (B) on HCT 116 CRC cells. Cells were seeded in 96-well plates at a density of 1×10^4 cells/well and cultured for 12 h. Following this, cells were treated with NPs loaded with increasing amounts of peptides (from 0.08 to 5 μM) for 24, 48, and 72 h. Then, cell viability was measured by the MTT assay. Bars represent the mean of triplicate experiments; error bars represent the standard deviation. *$p < 0.05$; **$p < 0.01$; ***$p < 0.001$ *vs* control cells set at 100%.

caused a reduction of cell viability of ∼70% at the same concentration and time point.

Of note, NPs/**9** reduced cell viability by 50% already after 48 h at 2.50 μM (Figure 4B). This higher activity could be clearly related to the lower IC_{50} of **9** compared to **3**, as previously found. NPs/**9** cytotoxic activity was also confirmed in SW48 and RKO CRC cell lines (Figure S6). In light of these observations, we focused our study on NPs loaded with **9**.

First, we examined the intracellular uptake of **9** in the HCT 116 cell line. To this purpose, cells were incubated with NPs loaded with **9-FITC** (4 μM) for 6 and 24 h. The fluorescence intensity of internalized **9-FITC** was measured by fluorimetry. As shown in Figure S7, the treatment with NPs/**9** was associated with an increasing time-dependent cellular uptake of **9**, according to the *in vitro* release of peptide **9** from NPs.

In order to verify the effect of **9** on p53 protein levels, we performed Western blotting experiments upon NPs/**9** treatment in HCT 116 cells. As expected, NPs/**9** caused a significant increase in p53 levels associated with a strong increment of its main downstream target p21 compared to control cells (Figures S8 and S9). These results confirmed the ability of **9** to enhance p53 stabilization, with consequent p53 transcriptional activation. These data are further corroborated by the evidence that **9** is able to induce apoptosis (see Figure S10).

Next, we investigated the cytotoxic effect of **9** in combination with 5-FU. To this aim, cells were incubated with NPs loaded with 5-FU alone or in combination with **9** from 24 to 72 h, and then, cell viability was assessed by the MTT assay (Figure 5). Our results showed that NPs/5-FU and NPs/5-FU/**9**

https://doi.org/10.1021/acs.jmedchem.3c01312
J. Med. Chem. 2024, 67, 1812−1824

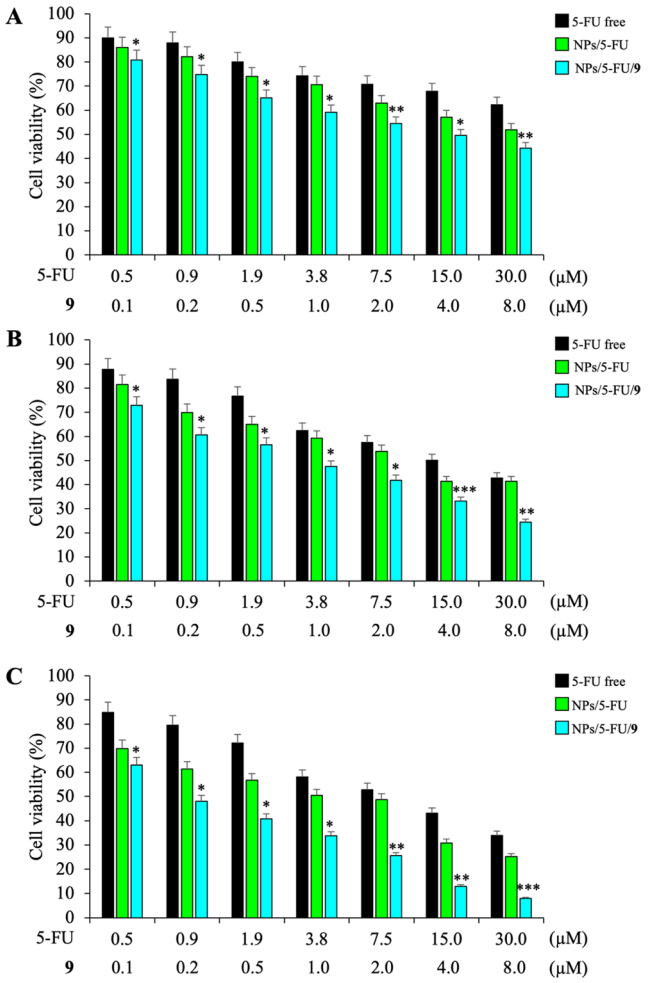

Figure 5. Cytotoxic effect of NPs loaded with 5-FU alone or in combination with **9** on HCT 116 cells. Cells were seeded in 96-well plates at a density of 1×10^4 cells/well and cultured for 12 h. Following this, cells were treated with NPs loaded with increasing amounts of 5-FU (from 0.5 to 30.0 μM) and/or **9** (from 0.1 to 8.0 μM) for 24 h (A), 48 h (B), and 72 h (C). Then, cell viability was measured by the MTT assay. Bars represent the mean of triplicate experiments; error bars represent the standard deviation. *$p < 0.05$; **$p < 0.01$; ***$p < 0.001$ *vs* NPs/5-FU.

consistently inhibit cell proliferation in a time- and dose-dependent manner since evident effects on the cell viability were observed mostly 48 and 72 h after treatment.

Specifically, NPs/5-FU had a greater cytotoxic effect than free 5-FU. In detail, we observed a 50% reduction in cell viability at 3.8 μM after 72 h of treatment with 5-FU loaded in NPs, whereas free 5-FU requires a concentration of 7.5 μM to achieve the same effect (Figure 5C). Additionally, the presence of **9** significantly increased the cytotoxic activity of NPs/5-FU. In fact, a 50% reduction in cell viability was observed at 3.8 and 0.9 μM 5-FU after 48 and 72 h of treatment, respectively (Figure 5B,C).

Overall, our findings suggest that NPs/5-FU/**9** combined therapy may be a promising treatment for CRC due to peptide **9**'s ability to enhance the cytotoxic effect of 5-FU.

Effect of NPs/5-FU/9 on Apoptosis and rRNA Processing. In order to investigate whether the combination of 5-FU and **9** decreased cell survival by inducing apoptosis, we carried out apoptosis analysis by flow cytometry. To this aim, cells were treated with 5-FU free, NPs/5-FU, or NPs/5-FU/**9**; after 72 h, the degree of apoptosis was determined with Annexin V-Alexa Fluor 488/PI dual staining (Figure 6A,B). As expected, treatment with 5-FU induces cell death, mainly by necrosis. In

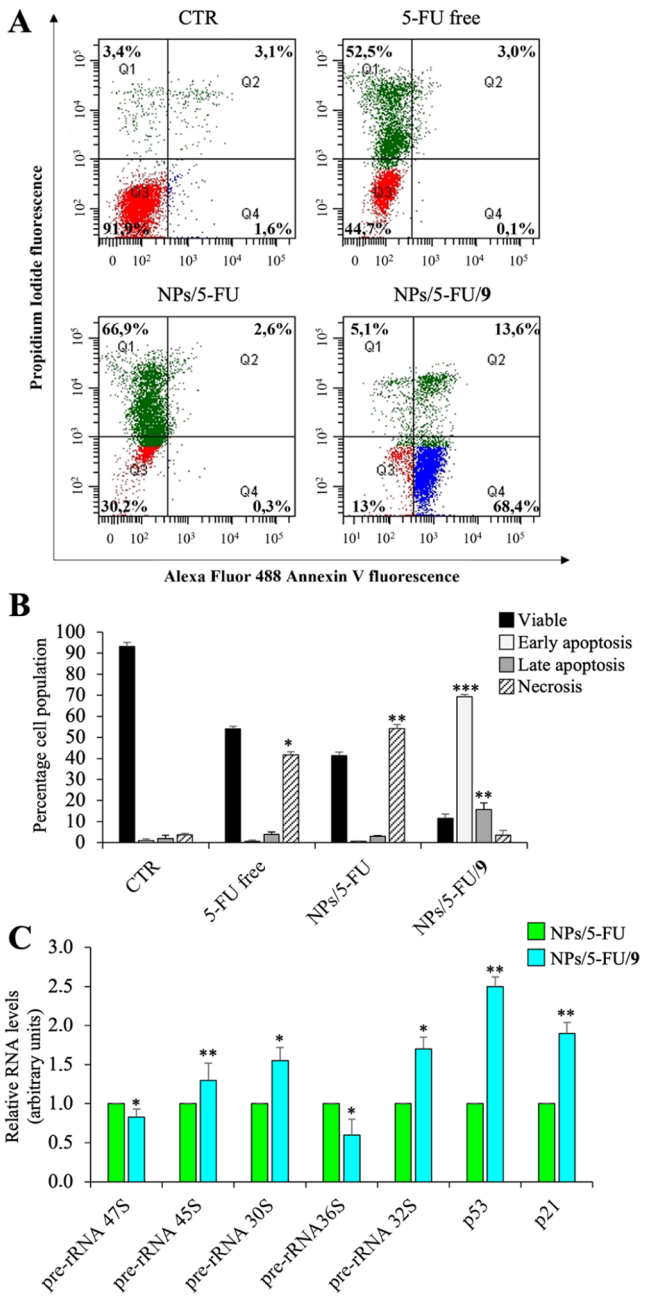

Figure 6. Effect of NPs/5-FU/**9** on apoptosis and rRNA processing. (A) Representative flow cytometry dot blots with double Annexin V-Alexa Fluor 488/PI staining for HCT 116 cells treated with free 5-FU (15 μM) or NPs loaded with 5-FU (15 μM) alone or a combination of 5-FU (15 μM) and **9** (4 μM) for 72 h. (B) The bar diagram shows the percentage of viable cells (Annexin V/PI negative), early apoptotic cells (Annexin V positive/PI negative), late apoptotic cells (Annexin V/PI positive), and necrotic cells (Annexin V negative/PI positive). Each bar represents the mean of triplicate experiments; error bars represent the standard deviation. For each sample, at least 2×10^4 events were analyzed. (C) Relative expression levels of rRNA from HCT 116 cells treated with 5-FU alone (15 μM) or in combination with **9** (4 μM) for 48 h. Then, the total RNA was extracted and analyzed by RT−qPCR with primers specific for indicated genes (Table 3). Bars represent the mean of triplicate experiments; error bars represent the standard deviation. *$p < 0.05$; **$p < 0.01$; ***$p < 0.001$ *vs* control cells.

https://doi.org/10.1021/acs.jmedchem.3c01312
J. Med. Chem. 2024, 67, 1812−1824

particular, we found 53 and 70% necrotic cells after 5-FU free and NPs/5-FU treatments, respectively. Surprisingly, treatment of cells with NPs/5-FU/**9** resulted in the induction of the apoptotic process. Specifically, following NPs/5-FU/**9** treatment, 70% of early apoptotic cells and 15% of late apoptotic cells were observed (Figure 6A,B). These data demonstrated the efficacy of **9** to enhance the cytotoxic effect of 5-FU in CRC cells by inducing apoptosis. This finding is very interesting in terms of combined 5-FU and peptide **9** therapy. In fact, it is well-known that phagocytosis removes apoptotic cells, preventing the induction of inflammatory responses and tissue damage. In contrast, necrosis-induced cell death activates the host's inflammatory response to the released cellular contents, causing additional tissue damage.[34]

The efficiency of rRNA processing is considered the most prominent hallmark of nucleolar stress activation, which occurs in response to a variety of chemotherapeutic drugs.[35] In the nucleolus, ribosomal genes are transcribed by RNA polymerase I to generate the pre-rRNA 47S, a single transcript that is then cleaved and processed to generate the mature 28S, 18S, and 5.8S rRNAs.[35] To understand the molecular mechanism underlying the cytotoxic activity of NPs/5-FU/9, and in particular, if the presence of 9 could influence the activation of 5-FU-induced p53-dependent nucleolar stress, we analyzed the expression profile of specific rRNA precursors (pre-rRNAs).

To this aim, cells were treated with NPs/5-FU and NPs/5-FU/**9** for 48 h. Then, total RNA was extracted from cell lysates, and the relative abundance of 47S, 45S, 30S, 32S, and 36S pre-rRNAs was determined by RT-qPCR with specific primers (Table 3).[36] As shown in Figure 6, the exposure of cells to NPs/5-FU/**9** caused an increase of 45S, 30S, and 32S pre-rRNAs levels compared to those observed upon NPs/5-FU treatment, whereas the expression levels of 47S and 36S pre-rRNAs decreased (Figure 6C). Of note, the treatment of cells was also associated with the increase of p53 and p21 expression according to the induction of apoptosis (Figure 6C). Altogether, these findings demonstrated the activation of the nucleolar stress response upon NPs/5-FU/**9** treatment.

Overall, our findings suggest that HA-coated NPs target HCT 116 cells, causing 5-FU and **9** to be released into the cell. We discovered a change in rRNA processing under this condition, which resulted in the activation of the nucleolar stress response. Simultaneously, peptide **9** disrupts the MDM2/4 heterodimer, resulting in p53 accumulation. These events eventually resulted in an increase in apoptosis, which promoted tumor cell death.

Table 3. Sequence of Oligonucleotides Used in RT-qPCR Analysis

gene	sequence
β-actin	forward: 5′−CCAACCGCGAGAAGATGA−3′
	reverse: 5′−CCAGAGGCGTACAGGGATAG−3′
p21	forward:5′−CCTCAAATCGTCCAGCGACCTT−3′
	reverse:5′−CATTGTGGGAGGAGCTGTGAAA−3′
p53	forward: 5′ − AGGCCTTGGAACTCAAGGAT − 3′
	reverse: 5′ − TGAGTCAGGCCCTTCTGTCT − 3′
pre-rRNA 47S	forward: 5′ − GCTGACACGCTGTCCTCTG− 3′
	reverse: 5′ − ACGCGCGAGAGAACAGCAG− 3′
pre-rRNA 45S	forward: 5′ − GCCTTCTCTAGCGATCTGAGAG−3′
	reverse: 5′−CCATAACGGAGGCAGAGACA−3′
pre-rRNA 36S	forward: 5′−GCGGAGGTTTAAAGACCC−3′
	reverse: 5′−CCAGACGAGACAGCAAAC−3′
pre-rRNA 32S	forward: 5′−GTCAGCGGAGGAGAAGAA−3′
	reverse: 5′−CTCGATCAGAAGGACTTGG−3′
pre-rRNA 30S	forward: 5′−CCTCTGACGCGGCAGACAGC−3′
	reverse: 5′−CTCCAGGAGCACCGCAAGGG−3′

Molecular Modeling. To elucidate the binding mode of the most potent peptide **9**, molecular docking calculations have been performed with the aid of Glide[37] within the Schrödinger package. The peptide was docked along the MDM2 RING domain interface that interacts with MDM4. Results converged in a set of poses very similar to one another, with **9** adopting a β-strand conformation, superimposable to that of **1** (see Figure 1). This conformation ensured the formation of a β-barrel with MDM2 and is stabilized by two distinct interaction patterns. First, as depicted in Figure 7, the C-terminal Ile and Ala residues of **9** are securely anchored in a highly hydrophobic pocket of MDM2. This pocket, as mentioned earlier, plays a critical role in stabilizing the MDM2/MDM4 heterodimer. This strong binding is justified by the presence of several lipophilic contacts with the side chains of L430, P431, A434, L458, M459, and F490 residues, as well as the H-bond between the amide terminal cap of **9** and the K446 side chain. The importance of these hydrophobic contacts is highlighted by the lower activity of all of the COOH-term analogues (such as **2**−**5** and **10**−**13**). In fact, although these peptides could form a H-bond with the K446 side chain, their negatively charged tail hampers their proper accommodation and interaction within this hydrophobic hot-spot-core of MDM2.

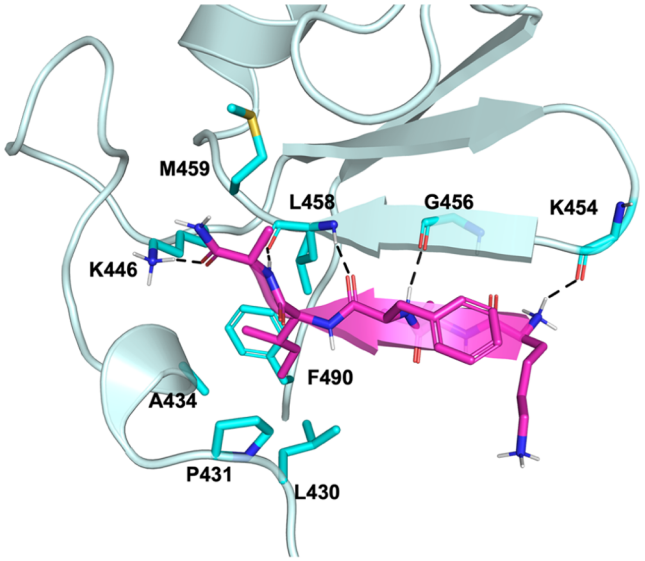

Figure 7. Lowest energy binding pose for the **9**/MDM2 complex (PDB code: 2VJF).[25] **9** residues are shown in magenta sticks and cartoon representations. Cyano stick representation is employed for MDM2 residues involved in hydrogen bonds (highlighted in black dashed lines) with **9**, while the rest of the protein is shown as light blue cartoon.

On the other hand, the β-strand conformation of **9** is also steadied by five H-bonds between **9** and the MDM2 counterpart (a detailed list of all of the formed hydrogen bond couples is reported in Table S1). The acetylation (**5**) and/or the elongation (**6**−**8** and **14**−**17**) at the N-terminus causes the loss of the last H-bond with K454 so that the acetyl-capped analogues of **9**, as well as all of the longer peptides, showed higher IC_{50} with respect to **9**.

https://doi.org/10.1021/acs.jmedchem.3c01312
J. Med. Chem. 2024, 67, 1812−1824

In line with these observations, docking calculations of **5** and **17** (see the binding mode of the latter in Figure S11) show that, in order to stabilize the β-strand conformation forming five H-bonds, these peptides are forced to completely flip themselves and arrange the charged C-terminal Lys into the hydrophobic core of MDM2 (see also the superposition with **9**, Figure S11), with the loss of the many aforementioned hydrophobic contacts. This, in analogy with the other cases, explains their lower affinity toward MDM2.

Therefore, the suggested binding model, featuring a well-structured hydrogen bond pattern and interactions within the hydrophobic hot-spot core of the MDM2 protein, provides a microscopic explanation for the strong potency of **9**. Also, it offers a molecular-level rationalization of the activity trends reported in Table 1.

Furthermore, the analysis of **9** in complex with the MDM2 RING domain interface paves the way for a rational optimization. Particularly, while the C-terminal Ala residue lies in a small pocket, the near Ile side chain is fitted in a deep hydrophobic tunnel. The shape of this pocket and the presence of F490 suggest the possibility to accommodate longer hydrophobic chains with an aromatic end at this position. On the other side, the central Phe and Val side chains of **9** could be shrunk to smaller hydrophobic side chains, in order to favor a tighter packing of the β-barrel with MDM2 and to strengthen the aforementioned H-bond pattern.

CONCLUSIONS

The current study has presented a library of peptides capable of disrupting the MDM2/MDM4 heterodimer, with two of them, namely, **3** and **9**, demonstrating 10-fold greater potency compared to the only reference compound available to date. To address their rapid degradation in the serum environment and facilitate their release into cells, a specialized nanoparticle delivery system was developed. This delivery system had already shown a remarkable ability to efficiently load and precisely deliver multiple drugs into CRC cells. When loaded into these nanoparticles, the most active compounds have effectively reduced the cell proliferation of CRC cells. Furthermore, in-depth biological investigations have revealed that peptide **9** has the ability to enhance 5-FU-induced p53-dependent nucleolar stress and trigger apoptosis in CRC cells. This breakthrough paves the way for a novel therapeutic strategy to treat CRC and overcome drug resistance. In summary, disrupting the MDM2/MDM4 heterodimer has proven to be a potent approach for reactivating p53, which is essential for sensitizing cancer cells to 5-FU and reinvigorating apoptosis. This approach offers a promising solution with a favorable safety profile, addressing the primary limitations associated with conventional MDM2 inhibitors.

EXPERIMENTAL SECTION

Materials and General Procedures. Hyaluronan (HA, < 10 kDa) was a kind gift of Magaldi Life S.r.l. (Italy). Poly(lactic-*co*-glycolic) acid (PLGA) (D,L-lactic, 50:50 Resomer RG 504, inherent viscosity 0.16−0.24 dL/g) was obtained from Boehringer Ingelheim (Germany). 5-Fluorouracil (5-FU), polyethylenimine (PEI, 25 kDa branched), poloxamer 188 (Pluronic F68), sodium acetate, sodium chloride, hexadecyltrimethylammonium bromide sodium hydroxide, and copper(II) sulfate were purchased from Sigma-Aldrich (St. Louis, MO). Formic acid, acetic acid, ethanol, and acetone were purchased from Carlo Erba Reagents (Italy). All buffers and solutions were prepared with ultrahigh quality water. All reagents were of the purest commercial grade.

The N^{a}-Fmoc-protected amino acids, such as Fmoc-Leu, Fmoc-Val, Fmoc-Ile, Fmoc-Lys(Boc), Fmoc-Phe, and Fmoc-Ala, were acquired from GL Biochem Ltd. (Shanghai, China). *N*,*N*-diisopropylethylamine (DIEA), piperidine, and trifluoroacetic acid (TFA) were purchased from Iris-Biotech GmbH. Coupling reagents, such as *N*,*N*,*N*′,*N*′-tetramethyl-*O*-(1*H*-benzotriazol-1-yl) uranium hexafluorophosphate (HBTU) and 1-hydroxybenzotriazole (HOBt), were commercially obtained by GL Biochem Ltd. (Shanghai, China). The solid supports [2-chlorotrityl chloride (2-CTC), 1.70 mmol/g as loading substitution or Rink amide, 0.72 mmol/g as loading substitution] were purchased by Iris-Biotech GMBH. Anhydrous solvents [*N*,*N*-dimethylformamide (DMF), dichloromethane (DCM)], acetic anhydride (Ac_2O), (1-cyano-2-ethoxy-2-oxoethylidenaminooxy)dimethylamino-morpholino-carbenium hexafluorophosphate (COMU), and ethyl cyano-(hydroxyimino)acetate (Oxyma Pure) were obtained from Merck/Sigma-Aldrich. Moreover, peptide synthesis solvents, such as *N*,*N*-dimethylformamide (DMF), dichloromethane (DCM), methanol (MeOH), diethyl ether (Et_2O), water, and acetonitrile (MeCN), for HPLC were reagent grade and acquired from commercial sources (Sigma-Aldrich and VWR) and used without further purification.

Purification of peptides was performed by RP-HPLC (Shimadzu Preparative Liquid Chromatograph LC-8A) equipped with a preparative column (Phenomenex Kinetex C18 column, 5 μm, 100 Å, 150 mm × 21.2 mm) using linear gradients of MeCN (0.1% TFA) in water (0.1% TFA) from 10 to 90% over 30 min with a flow rate of 10 mL/min and ultraviolet (UV) detection at 220 nm. Final products were obtained by lyophilization of the appropriate fractions after removal of MeCN by rotary evaporation. Analytical ultra-high-performance liquid chromatography (UHPLC) (Shimadzu Nexera Liquid Chromatograph LC- 30AD) analyses to assess the purity of peptides **2**−**17** were performed on a Phenomenex Kinetex reversed-phase column (C18, 5 μm, 100 Å, 150 mm × 4.6 mm) with a flow rate of 1 mL/min using a gradient of MeCN (0.1% TFA) in water (0.1% TFA) from 10 to 90% over 15 min and UV detection at 220 nm. All compounds examined for biological activity were purified to >97% (Figures S9−S24), and the correct molecular ions were confirmed by an HRMS spectrometer (LTQ Orbitrap).

Peptide Synthesis. The synthesis of peptides was performed by using ultrasound-assisted solid-phase peptide synthesis (US-SPPS) *via* the Fmoc/*t*-Bu orthogonal protection strategy. The ultrasonic conditions were used as previously described.[27] Peptides were assembled on 2-chlorotrityl chloride (2-CTC) (0.1 mmol; 1.70 mmol/g as loading substitution) or Rink amide (0.1 mmol; 0.72 mmol/g as loading substitution) resins depending on the C-terminal target as carboxylic acid (peptides **2**−**5** and **10**−**13**, series A and C) or amide (peptides **6**−**9** and **14**−**17**, series B and D), respectively. The resin was first placed in a polypropylene tube (ISOLUTE SPE filtration column by Biotage, Uppsala, Sweden) and swollen in DMF for 30 min. Then, the first attachment was carried out according to two different procedures, as elsewhere.[38,39]

*Peptides **2**−**5** and **10**−**13**, Series A and C.* A solution of Fmoc-Ala (1 equiv) and *N*,*N*-diisopropylethylamine (DIPEA) (2 equiv) in anhydrous DMF was added to the resin, and the resulting suspension was shaken overnight at room temperature. The residual chloride reactive groups were then capped by adding a previously mixed solution of DIEA/DCM/MeOH (10:85:5) and allowing gentle shaking for 1 h.

*Peptides **6**−**9** and **14**−**17**, Series B and D.* The resin, stored as Fmoc-protected, was treated with 20% piperidine in DMF solution (5 min × 1, 25 min × 1), and then the coupling with the first residue Fmoc-Val (3 equiv) was achieved by using HBTU (3 equiv)/HOBt (3 equiv) and DIPEA (6 equiv) on an automated shaker for 2 h at rt.

At this point, reactions proceeded in the same way for all series. To remove the Fmoc group, 20% piperidine in DMF solution was added to the resin, and a tube reactor was then placed in an ultrasonic bath (0.5 + 1 min). Otherwise, the couplings were carried out by treatment with a solution of the Fmoc-amino acid (2 equiv), COMU (2 equiv), Oxyma Pure (2 equiv), and DIPEA (4 equiv) in DMF and by exposing the resin to the ultrasonic irradiation for 5 min. After each Fmoc-deprotection and coupling step, filtering and washing of the resin were executed (3 × 2 mL of DMF; 3 × 2 mL of DCM). The *N*-terminal primary amine of

https://doi.org/10.1021/acs.jmedchem.3c01312
J. Med. Chem. 2024, 67, 1812−1824

resin-bound sequences of series A and D (peptides **2**−**5** and **14**−**17**) was acetylated by treating with a solution of Ac_2O (2 equiv) and DIPEA (4 equiv) in DMF, and the reactor was shaken on an automated shaker for 30 min at rt. In the construction of peptide **9** labeled with fluorescein, used in the release studies, the N-terminal of peptide **9** was treated with fluorescein isothiocyanate (FITC) prior to the introduction of a spacer. To monitor the US-SPPS reactions, the colorimetric Kaiser test was used for the detection of solid-phase bound amines. Upon construction of the target sequence, peptides were finally cleaved by treating with a 95% TFA solution on a magnetic stirrer plate (200 rpm), recovered by precipitation with chilled anhydrous Et_2O (10 mL), and then centrifuged (6000 rpm × 15 min). The supernatants were carefully removed, and the resulting white to pale beige-colored amorphous solids were dried and dissolved in water/acetonitrile (9:1) for analysis by reversed-phase HPLC. All compounds examined for biological activity were purified to >97%, and prior to their use for biological assays, the correct molecular ions were confirmed.

Dissociation Studies of Native MDM2/MDM4 Complex. Starting from previously published papers, we fine-tuned an MDM2/MDM4 dissociation assay.[18,40] In particular, the MDM2/MDM4 complex dissociation assay was carried out in the MCF-7 cell line, expressing high levels of MDM2/4,[28] by a homemade immunoenzymatic assay, similar to others previously reported.[41−43] In brief, wells were precoated with an anti-MDM4 (#A300−287A-T, Bethyl Laboratories Inc.) antibody, diluted 1:500 in poly ornithine, and left overnight at room temperature. MCF-7 cells were suspended in lysis buffer (20 mM Tris−HCl, 137 mM NaCl, 10% glycerol, 1% NONIDET40, and 2 mM EDTA, pH 8) containing 1% of the protease inhibitor cocktail (Merck). Fifteen micrograms of cell lysates was treated with different concentrations of the tested compounds for 10 min at room temperature and then transferred to the precoated wells for 90 min. After extensive washes, each well was incubated with 1% BSA to block nonspecific sites and then treated for 90 min with an anti-MDM2 antibody (#MABE281, Merck). Then, the wells were washed and treated with a secondary HRP-conjugate antibody. The TMB substrate kit (Thermo Fisher Scientific) allowed colorimetric quantification of the complexes. Absorbance was measured at 450 nm. Dose−response curves were derived with Graph Pad Prism 7 software, from which IC_{50} values were obtained. The antibodies were chosen taking into account the interaction zones between MDM2 and MDM4.[40] **1** was used as the reference compound.

Molecular Docking. The **9**/MDM2, **5**/MDM2, and **17**/MDM2 complexes were obtained starting from the crystallographic structure of the MDM2/MDM4 heterodimer complex (PDB code: 2VJF).[25] First, to model **9**, MDM4 was cut from residue E428 to residue I485, and then the N-terminus was left free; the C-terminus was capped with a *N*-methylamide (NME) group. The same cut was made to models **5** and **17**; then, this time, the N-terminus was capped with an acetyl group (ACE), while the C-terminus was left free in the case of **5** and capped with a *N*-methylamide (NME) group in the case of **17**. The peptides were subjected to preparation by using the LigPrep[44] module included in Maestro[45] (Version 12.7.156), the interface for Schrödinger's molecular modeling platform, employing the OPLS2005[46] force field. The Epik[47] module of Maestro was used to evaluate the pK_a at pH = 7 and properly describe their protonation state. Accordingly, the free **9** N-terminus was considered as positively charged. The so-obtained **9** presented a net charge of +2, while **5** and **17** carried net charges of 0 and +1, respectively.

Regarding MDM2, it was prepared with the Protein Preparation Wizard feature of Maestro. The hydrogens were added to the protein and missing side chains were added by using the Prime[48] module of Maestro; crystallographic water molecules were deleted, and a residue protonation state, according to a neutral pH, was assigned evaluating their pK_a with the Propka program included in Maestro.[45] The N-terminal and C-terminal residues were capped with acetyl (ACE) and *N*-methylamide (NME) groups, respectively. Then, a relaxation procedure was performed by running a restrained minimization only on the initially added hydrogen atoms, according to the OPLS2005 force field.

To perform docking simulations with Glide[37] software, a receptor grid was built based on the **9**/MDM2 complex. More in detail, the grid box was centered on the **9** or **17** centroid and a box of ∼10 Å × 10 Å × 10 Å in the three-dimensional Cartesian coordinate system was generated. The volume of this box represented the space in which the ligand center was confined during the site point search and was a measure of the effective size of the search space. An outer box ∼20 Å larger than the inner box in each of the three dimensions represented the volume, in which all of the peptide atoms were confined. Single precision peptide docking simulations were performed and the best 20 poses were chosen for further optimization. In all of the simulations, MDM2 was kept fixed, the peptides were treated as flexible, and no other constraints were added.

Preparation and Characterization of NPs. NPs were prepared by solvent diffusion of an organic phase (2 mL) in an aqueous phase (4 mL of water with Pluronic F68 0.1%). We prepared unloaded NPs (without drugs), NPs loaded with 5-FU (NPs/5-FU), NPs loaded with a peptide (NPs/**3** and NPs/**9**), and NPs loaded with 5-FU and a peptide simultaneously (NPs/5-FU/**3** and NPs/5-FU/**9**). The organic phase was prepared by dissolving 10 mg of PLGA 504 and 0.5 mg of PEI in 2 mL of acetone. 5-FU and/or **3** or **9** (200 mL of a 2.5 mg/mL ethanol solution) were added to the organic phase in the case of loaded NPs. The organic phase was added dropwise to the water phase with magnetic stirring. After solvent removal under reduced pressure and room temperature, PLGA dispersion was splitted into 4 eppendorf tubes, centrifuged (5000*g* for 20 min) for washing, and redispersed in 1 mL of water. Final NPs were obtained by adding 100 μL of HA to water (1 mg/mL) in each eppendorf. The interval between each addition was kept constant for 15 min. The hydrodynamic diameter (DH), polydispersity index (PDI), and zeta potential (ζ) of NPs were determined on a Zetasizer Nano ZS instrument (Malvern Instruments Ltd.). Results are reported as the mean of three separate measurements of three different batches ± standard deviation ($n = 9$). The yield of the NP production process was evaluated on an aliquot of NP dispersion by weighting the solid residue after freeze-drying. Results are expressed as the ratio of the actual NP weight to the theoretical polymer or polymer + drug weight × 100 ± standard deviation ($n = 3$). The NP morphology was examined by transmission electron microscopy (TEM) (CM 12 Philips, Eindhoven, The Netherlands) after staining samples with a 2% w/v phosphotungstic acid solution and scanning electron microscopy (Phenom Prox).

PEI and HA Amount in NPs. PEI was quantified by a colorimetric method developed previously.[30] To evaluate the amount of PEI in NPs, 0.5 mg of freeze-dried NPs was treated with 1 mL of 1 M NaOH and stirred overnight. The sample (0.5 mL) was diluted with 0.5 mL of 1 M acetic acid. The resulting solution (0.5 mL) was added to 1 mL of 0.1 M acetate buffer at pH 5.4 and complexed with 0.25 mL of a copper(II) sulfate water solution (0.1% w/v). The absorbance value of each solution was recorded at 281 nm (UV 1800, Shimadzu, Japan). A calibration curve was constructed in the same condition in the PEI concentration range of 15−400 μg/mL. To evaluate the extent of HA adsorption onto NPs, we performed a method previously developed.[30] Briefly, 0.5 mg of NPs was centrifuged at 13,000*g* for 15 min, and the supernatant was withdrawn and freeze-dried. The solid residue was then dissolved in 1 mL of 0.2 M acetate buffer (0.2 M sodium acetate and 0.15 M sodium chloride) at pH 6. Thereafter, 2 mL of a cetyltrimethylammonium bromide reagent (2 g of sodium hydroxide and 1 g of hexadecyltrimethylammonium bromide in 100 mL of water) was added, and the sample was analyzed at 350 nm. A calibration curve was constructed in the HA concentration range of 10−200 μg/mL.

5-FU and Peptide Actual Loading in NPs. 5-FU loading inside NPs was assessed by placing 0.5 mg of freeze-dried NPs in 500 μL of DCM and 500 μL of water. Thereafter, the sample was mixed vigorously and centrifuged at 2000*g* for 5 min. The amount of 5-FU in the water phase was analyzed by HPLC as previously described[31] on a Shimadzu apparatus equipped with an LC-10ADvp pump, an SIL-10ADvp autoinjector, an SPD-10Avp UV/visible (UV−vis) detector, and a C-R6 integrator. The analysis was performed on a Synergy Hydro C18 column (25 × mm^2). The mobile phase was a 100% (v/v) mixture of water and formic acid (99:1) pumped at a flow rate of 1 mL/min. The

https://doi.org/10.1021/acs.jmedchem.3c01312
J. Med. Chem. 2024, 67, 1812−1824

UV detector was set at 285 nm. A calibration curve of 5-FU in water was constructed in the concentration range 1−100 μg/mL.

The loading of peptides inside NPs was evaluated by placing 1 mg of freeze-dried NPs in 500 μL of DCM and 500 μL of EtOH. Thereafter, the sample was mixed vigorously and centrifuged at 2000*g* for 5 min. The amount of peptides in ethanol was analyzed through the Pierce Quantitative Fluorometric Peptide Assay. Briefly, 10 mL of the samples was mixed with 90 mL of the Pierce reagent and the emission fluorescence read at 500 nm (l_{ex} = 405 nm). As a control, the fluorescence of NPs/5-FU was analyzed in the same conditions. A calibration curve of both peptides in EtOH was constructed in the concentration range of 20−1000 μg/mL.

Release Studies of 5-FU and Peptide 9 from NPs. *In vitro* release of 5-FU and **9-FITC** from NPs was assessed in 10 mM phosphate buffer containing NaCl (137 mM) and KCl (2.7 mM) at pH 7.4 (PBS) by a dialysis method. A known amount of NPs (1.25 mg) was dispersed in 0.5 mL of PBS and placed in a dialysis bag (MWCO = 3500 Da, Spectra/Por). The sample was plunged in 5 mL of PBS (sink condition) and kept at 37 °C. At selected time intervals, 1 mL of release medium was withdrawn and replaced with an equal volume of fresh medium. 5-FU quantitative analysis was performed as described above. **9-FITC** quantitative analysis was performed by spectrometry (λ = 425). Results are expressed as release % over time ± standard deviation of three experiments.

Peptide Serum Stability. Peptide serum stability was established by modification of elsewhere described methods.[49,50] In particular, 2 mM peptide stock solutions in water were mixed with human serum (from male AB plasma, USA origin, sterile-filtered; Merck/Sigma-Aldrich) to a final concentration of 500 μM [stock solution/human plasma (25:75, v/v)] and incubated at 37 ± 1 °C. At different time intervals (0, 0.5, 1, 2, and 3 h), 80 μL of aliquots was taken, and protease activity was stopped by adding 160 μL of acetonitrile (MeCN). The produced cloudy suspension was cooled to 4 °C for 30 min and then centrifuged at 12,000 rpm for 10 min to remove the serum proteins. Then, the supernatant was analyzed by analytical UHPLC (Shimadzu Nexera Liquid Chromatograph LC-30AD), which was equipped with a Phenomenex Kinetex reversed-phase column (C18, 5 μm, 100 Å, 150 × 4.6 mm^2) with a flow rate of 1 mL/min using a gradient of MeCN (0.1% TFA) in water (0.1% TFA) from 0 to 60% over 20 min and UV detection at 220 nm. The proteolytic stability assay was repeated in triplicate. The percentage of intact peptides at different time intervals (Figure S3) was monitored by calculating the peak area of the chromatograms resulting from RP-HPLC analyses.

Stability of NPs in Fetal Bovine Serum. Stability of NPs in the presence of FBS was assessed by dynamic light scattering (DLS) measurements and turbidimetry analyses. 200 mL of NPs (0.5 mg) was mixed with 800 mL of FBS (10% in water). At different time points (0, 24, and 72 h), size, z, and scattering (absorbance at 500 nm) of NPs in FBS were monitored. Control samples of FBS and NPs in water were run as the control.

Cell Culture and Treatments with NPs. HCT 116, SW48, and RKO cells (American Type Culture Collection, (ATTC) Manassas, Virginia) were cultured in Dulbecco's modified Eagle's medium (DMEM), supplemented with 10% fetal bovine serum (FBS), 2 mM L-glutamine, and 50 U/ml penicillin−streptomycin under a humidified atmosphere of 5% CO_2 at 37 °C.

Treatments of cells were performed by replacing the culture medium with those containing different concentrations of 5-FU or NPs loaded with 5-FU, **3**, **9**, or a combination of 5-FU and **9** from 24 to 72 h.

MTT Assay. Cells were seeded onto 96-well plates at a density of 1 × 10^4 cells/well and treated with different concentrations of NPs from 24 to 72 h. Then, cell viability was determined using the MTT assay, as previously reported.[51] A pool of three different sets of experiments was performed. Error bars represent the standard deviation.

Cell Death Assay. Apoptosis analysis was performed as previously described.[52] Briefly, HCT 116 cells were seeded into 60 mm tissue culture plates at a confluency of about 50−60%. Then, cells were treated with 5- FU, NPs loaded with 5-FU alone, or in combination with **9**. After 72 h, the cells were stained using the Tali Apoptosis Kit, Annexin V-Alexa Fluor 488, and propidium iodide (PI; Life Technologies, Carlsbad, CA). Cell apoptosis was analyzed using a BD FACS CantoII Cytometer (BD Biosciences, San Jose, CA) and Diva software (v6.x).

RT-qPCR. Total RNA was isolated from cells, as previously described.[53] RNA was retrotranscribed using a SensiFASTTM cDNA Synthesis kit (Bioline, London, U.K.), and then, real-time PCR was carried out using a SensiFAST SYBERNo-ROX kit (Bioline, London, U.K.). The primers are indicated in Table 3. The comparative Ct method was used to calculate the relative abundance of mRNA and compared with that of β-actin expression.[54]

Intracellular Uptake of 9. The uptake of **9** was evaluated by measuring the incorporation of **9-FITC** into HCT 116 cells. Briefly, cells were plated at a density of 1 × 10^5 cells per well in 24-well plates and treated with NPs loaded with 9-FITC (4 μM) for 6 and 24 h. Then, cells were collected and analyzed by fluorimetry on a Cary Eclipse fluorescence spectrophotometer (Varian). Excitation and emission wavelengths were 495 and 519 nm, respectively.

Western Blotting Analysis. Western blot analysis was performed as previously reported.[56] The membranes were challenged with anti-p53, anti-p21 (Santa Cruz, Dallas, TX), and anti-GAPDH (Cell Signaling Technology, Danvers, MA). Proteins were visualized with an enhanced chemiluminescence detection reagent, according to the manufacturer's instructions (Elabscience, Houston, TX).

Statistical Analysis. Statistical comparisons were made as previously shown.[55]

■ ASSOCIATED CONTENT

Supporting Information

The Supporting Information is available free of charge at https://pubs.acs.org/doi/10.1021/acs.jmedchem.3c01312.

Calibration curve for MDM2/4 heterodimer dissociation assay (Figure S1); displacing curve of MDM2-MDM4 complex (Figure S2); serum stability of peptides **3** and **9** (Figure S3); SEM image of NPs (Figure S4); cytotoxic effect of NPs on HCT 116 cells (Figure S5); cytotoxic effect of NPs/**9** on SW48 and RKO colorectal cancer cells (Figure S6); intracellular uptake of **9-FITC** in HCT 116 cells (Figure S7); effect of NPs/**9** treatment on p53 and p21 expression in HCT 116 cells (Figure S8); full-length blots of Figure S8 (Figure S9); bar diagram of the effect of NPs/**9** on apoptosis analyzed by flow cytometry (Figure S10); hydrogen bond interactions between **9** and MDM2 (Table S1); superposition of **9** and **17** docking poses and 17/MDM2 binding mode (Figure S11); analytical data of peptides **2**−**17** (Table S2); HPLC chromatograms of peptides **2**−**17** (Figures S12−27) (PDF)

molecular formula strings (CSV)

Complex structure of **9** with MDM2 (PDB)

■ AUTHOR INFORMATION

Corresponding Authors

Claudia Conte − *Department of Pharmacy, University of Naples Federico II, 80131 Napoli, NA, Italy*; Email: claudia.conte@unina.it

Annapina Russo − *Department of Pharmacy, University of Naples Federico II, 80131 Napoli, NA, Italy*; orcid.org/0000-0002-7509-3702; Email: annapina.russo@unina.it

Valeria La Pietra − *Department of Pharmacy, University of Naples Federico II, 80131 Napoli, NA, Italy*; orcid.org/0000-0001-8096-8377; Email: valeria.lapietra@unina.it

Authors

Francesco Merlino − *Department of Pharmacy, University of Naples Federico II, 80131 Napoli, NA, Italy*; orcid.org/0000-0002-9607-229X

https://doi.org/10.1021/acs.jmedchem.3c01312
J. Med. Chem. 2024, 67, 1812−1824

Annalisa Pecoraro − *Department of Pharmacy, University of Naples Federico II, 80131 Napoli, NA, Italy*
Giuseppe Longobardi − *Department of Pharmacy, University of Naples Federico II, 80131 Napoli, NA, Italy*
Greta Donati − *Department of Pharmacy, University of Naples Federico II, 80131 Napoli, NA, Italy*
Francesco Saverio Di Leva − *Department of Pharmacy, University of Naples Federico II, 80131 Napoli, NA, Italy; Department of Pharmacy, University of Pisa, 56126 Pisa, PI, Italy;* orcid.org/0000-0002-2294-0656
Chiara Brignola − *Department of Pharmacy, University of Naples Federico II, 80131 Napoli, NA, Italy;* orcid.org/0000-0002-4842-6532
Rebecca Piccarducci − *Department of Pharmacy, University of Pisa, 56126 Pisa, PI, Italy*
Simona Daniele − *Department of Pharmacy, University of Pisa, 56126 Pisa, PI, Italy*
Claudia Martini − *Department of Pharmacy, University of Pisa, 56126 Pisa, PI, Italy;* orcid.org/0000-0001-9379-3027
Luciana Marinelli − *Department of Pharmacy, University of Naples Federico II, 80131 Napoli, NA, Italy;* orcid.org/0000-0002-4084-8044
Giulia Russo − *Department of Pharmacy, University of Naples Federico II, 80131 Napoli, NA, Italy*
Fabiana Quaglia − *Department of Pharmacy, University of Naples Federico II, 80131 Napoli, NA, Italy;* orcid.org/0000-0001-6223-0782

Complete contact information is available at: https://pubs.acs.org/10.1021/acs.jmedchem.3c01312

Author Contributions

[§]F.M. and A.P. contributed equally to this work. This manuscript was written through contributions of all authors. All authors have given approval to the final version of the manuscript.

Notes

The authors declare no competing financial interest.

■ ACKNOWLEDGMENTS

Research reported in this publication was supported by the Faculty of Pharmacy, University of Naples Federico II research under grant “Bando per la ricerca” 2020”.

■ ABBREVIATIONS USED

5-FU, 5-fluoruracil; COMU, (1-cyano-2-ethoxy-2-oxoethylidenaminooxy)dimethylamino-morpholino-carbenium hexafluorophosphate; CRC, colorectal cancer; DIPEA, *N,N*-diisopropylethylamine; FBS, fetal bovine serum; HA, hyaluronic acid; MDM2, murine double minute 2; MDM4, murine double minute 4; NPs, nanoparticles; PEI, polyethylenimine; (PLGA), poly(lactic-*co*-glycolic acid); rDNA, ribosomal DNA; rRNA, ribosomal RNA; US-SPPS, ultrasound-assisted solid-phase peptide synthesis

■ REFERENCES

(1) Global Cancer Observatory. https://gco.iarc.fr. (accessed on October 3, 2022).
(2) Costas-Chavarri, A.; Nandakumar, G.; Temin, S.; Lopes, G.; Cervantes, A.; Correa, M. C.; Engineer, R.; Hamashima, C.; Ho, G. F.; Huitzil, F. D.; Moghani, M. M.; Sharara, A. I.; Stern, M. C.; Teh, C.; Manjarrez, S. E. V.; Verjee, A.; Yantiss, R.; Shah, M. A. Treatment of Patients With Early-Stage Colorectal Cancer: ASCO Resource-Stratified Guideline. *J. Global Oncol.* **2019**, *5*, 1−19.
(3) Diesch, J.; Hannan, R. D.; Sanij, E. Perturbations at the ribosomal genes loci are at the centre of cellular dysfunction and human disease. *Cell Biosci.* **2014**, *4*, No. 43.
(4) Carotenuto, P.; Pecoraro, A.; Palma, G.; Russo, G.; Russo, A. Therapeutic Approaches Targeting Nucleolus in Cancer. *Cells* **2019**, *8*, No. 1090.
(5) (a) Sullivan, K. D.; Galbraith, M. D.; Andrysik, Z.; Espinosa, J. M. Mechanisms of transcriptional regulation by p53. *Cell Death Differ.* **2018**, *25*, 133−143. (b) Maietta, I.; Del Peschio, F.; Buonocore, P.; Viscusi, E.; Laudati, S.; Iannaci, G.; Minopoli, M.; Motti, M. L.; De Falco, V. p90RSK Regulates p53 Pathway by MDM2 Phosphorylation in Thyroid Tumors. *Cancers* **2023**, *15*, No. 121.
(6) Migliorini, D.; Danovi, D.; Colombo, E.; Carbone, R.; Pelicci, P. G.; Marine, J. C. Hdmx recruitment into the nucleus by Hdm2 is essential for its ability to regulate p53 stability and transactivation. *J. Biol. Chem.* **2002**, *277*, 7318−7323.
(7) Shvarts, A.; Bazuine, M.; Dekker, P.; Ramos, Y. F.; Steegenga, W. T.; Merckx, G.; van Ham, R. C.; van der Houven van Oordt, W.; van der Eb, A. J.; Jochemsen, A. G. Isolation and identification of the human homolog of a new p53-binding protein, Mdmx. *Genomics* **1997**, *43*, 34−42.
(8) Russo, A.; Russo, G. Ribosomal Proteins Control or Bypass p53 during Nucleolar Stress. *Int. J. Mol. Sci.* **2017**, *18*, No. 140.
(9) Hou, H.; Sun, D.; Zhang, X. The role of MDM2 amplification and overexpression in therapeutic resistance of malignant tumors. *Cancer Cell Int.* **2019**, *19*, No. 216.
(10) Atwal, G. S.; Kirchhoff, T.; Bond, E. E.; Montagna, M.; Menin, C.; Bertorelle, R.; Scaini, M. C.; Bartel, F.; Bohnke, A.; Pempe, C.; Gradhand, E.; Hauptmann, S.; Offit, K.; Levine, A. J.; Bond, G. L. Altered tumor formation and evolutionary selection of genetic variants in the human MDM4 oncogene. *Proc. Natl. Acad. Sci. U.S.A.* **2009**, *106*, 10236−10241.
(11) (a) Imanishi, M.; Yamamoto, Y.; Wang, X.; Sugaya, A.; Hirose, M.; Endo, S.; Natori, Y.; Yamato, K.; Hyodo, I. Augmented antitumor activity of 5-fluorouracil by double knockdown of MDM4 and MDM2 in colon and gastric cancer cells. *Cancer Sci.* **2019**, *110*, 639−649. (b) Raimundo, L.; Espadinha, M.; Soares, J.; Loureiro, J. B.; Alves, M. G.; Santos, M. M. M.; Saraiva, L. Improving anticancer activity towards colon cancer cells with a new p53-activating agent. *Br. J. Pharmacol.* **2018**, *175*, 3947−3962.
(12) Konopleva, M.; Martinelli, G.; Daver, N.; Papayannidis, C.; Wei, A.; Higgins, B.; Ott, M.; Mascarenhas, J.; Andreeff, M. MDM2 inhibition: an important step forward in cancer therapy. *Leukemia* **2020**, *34*, 2858−2874.
(13) Khoo, K. H.; Verma, C. S.; Lane, D. P. Drugging the p53 pathway: understanding the route to clinical efficacy. *Nat. Rev. Drug Discovery* **2014**, *13*, 217−236.
(14) Pant, V.; Xiong, S.; Iwakuma, T.; Quintas-Cardama, A.; Lozano, G. Heterodimerization of Mdm2 and Mdm4 is critical for regulating p53 activity during embryogenesis but dispensable for p53 and Mdm2 stability. *Proc. Natl. Acad. Sci. U.S.A.* **2011**, *108*, 11995−20000.
(15) Tan, B. X.; Liew, H. P.; Chua, J. S.; Ghadessy, F. J.; Tan, Y. S.; Lane, D. P.; Coffill, C. R. Anatomy of Mdm2 and Mdm4 in evolution. *J. Mol. Cell Biol.* **2017**, *9*, 3−15.
(16) Tang, Y.; Zhao, W.; Chen, Y.; Zhao, Y.; Gu, W. Acetylation is indispensable for p53 activation. *Cell* **2008**, *133*, 612−626.
(17) Huang, L.; Yan, Z.; Liao, X.; Li, Y.; Yang, I.; Wang, Z. G.; Zuo, Y.; Kawai, H.; Shadfan, M.; Ganapathy, S.; Yuan, Z. The p53 inhibitors MDM2/MDMX complex is required for control of p53 activity in vivo. *Proc. Natl. Acad. Sci. U.S.A.* **2011**, *108*, 12001−12006.
(18) Pellegrino, M.; Mancini, F.; Luca, R.; Coletti, A.; Giacche, N.; Manni, I.; Arisi, I.; Florenzano, F.; Teveroni, E.; Buttarelli, M.; Fici, L.; Brandi, R.; Bruno, T.; Fanciulli, M.; D'Onofrio, M.; Piaggio, G.; Pellicciari, R.; Pontecorvi, A.; Marine, J. C.; Macchiarulo, A.; Moretti, F. Targeting the MDM2/MDM4 interaction interface as a promising approach for p53 reactivation therapy. *Cancer Res.* **2015**, *75*, 4560−4572.

(19) Yu, M.; Wu, J.; Shi, J.; Farokhzad, O. C. Nanotechnology for protein delivery: Overview and perspectives. *J. Controlled Release* **2016**, *240*, 24−37.
(20) Kovalainen, M.; Monkare, J.; Riikonen, J.; Pesonen, U.; Vlasova, M.; Salonen, J.; Lehto, V. P.; Jarvinen, K.; Herzig, K. H. Novel delivery systems for improving the clinical use of peptides. *Pharmacol. Rev.* **2015**, *67*, 541−561.
(21) Ilangala, A. B.; Lechanteur, A.; Fillet, M.; Piel, G. Therapeutic peptides for chemotherapy: Trends and challenges for advanced delivery systems. *Eur. J. Pharm. Biopharm* **2021**, *167*, 140−158.
(22) Durán-Lobato, M.; Lopez-Estevez, A. M.; Cordeiro, A. S.; Dacoba, T. G.; Crecente-Campo, J.; Torres, D.; Alonso, M. J. Nanotechnologies for the delivery of biologicals: Historical perspective and current landscape. *Adv. Drug Delivery Rev.* **2021**, *176*, No. 113899.
(23) Zhao, H.; Lin, Z. Y.; Yildirimer, L.; Dhinakar, A.; Zhao, X.; Wu, J. Polymer-based nanoparticles for protein delivery: design, strategies and applications. *J. Mater. Chem. B* **2016**, *4*, 4060−4071.
(24) Kemp, J. A.; Shim, M. S.; Heo, C. Y.; Kwon, Y. J. "Combo" nanomedicine: Co-delivery of multi-modal therapeutics for efficient, targeted, and safe cancer therapy. *Adv. Drug Delivery Rev.* **2016**, *98*, 3−18.
(25) Linke, K.; Mace, P. D.; Smith, C. A.; Vaux, D. L.; Silke, J.; Day, C. L. Structure of the MDM2/MDMX RING domain heterodimer reveals dimerization is required for their ubiquitylation in trans. *Cell Death Differ.* **2008**, *15*, 841−848.
(26) Lijnzaad, P.; Argos, P. Hydrophobic patches on protein subunit interfaces: characteristics and prediction. *Proteins* **1997**, *28*, 333−343.
(27) Merlino, F.; Tomassi, S.; Yousif, A. M.; Messere, A.; Marinelli, L.; Grieco, P.; Novellino, E.; Cosconati, S.; Di Maro, S. Boosting Fmoc Solid-Phase Peptide Synthesis by Ultrasonication. *Org. Lett.* **2019**, *21*, 6378−6382.
(28) Graves, B.; Thompson, T.; Xia, M.; Janson, C.; Lukacs, C.; Deo, D.; Di Lello, P.; Fry, D.; Garvie, C.; Huang, K. S.; Gao, L.; Tovar, C.; Lovey, A.; Wanner, J.; Vassilev, L. T. Activation of the p53 pathway by small-molecule-induced MDM2 and MDMX dimerization. *Proc. Natl. Acad. Sci. U.S.A.* **2012**, *109*, 11788−11793.
(29) Daniele, S.; Taliani, S.; Da Pozzo, E.; Giacomelli, C.; Costa, B.; Trincavelli, M. L.; Rossi, L.; La Pietra, V.; Barresi, E.; Carotenuto, A.; Limatola, A.; Lamberti, A.; Marinelli, L.; Novellino, E.; Da Settimo, F.; Martini, C. Apoptosis therapy in cancer: the first single-molecule co-activating p53 and the translocator protein in glioblastoma. *Sci. Rep.* **2014**, *4*, No. 4749.
(30) Maiolino, S.; Moret, F.; Conte, C.; Fraix, A.; Tirino, P.; Ungaro, F.; Sortino, S.; Reddi, E.; Quaglia, F. Hyaluronan-decorated polymer nanoparticles targeting the CD44 receptor for the combined photo/chemo-therapy of cancer. *Nanoscale* **2015**, *7*, 5643−5653.
(31) Russo, A.; Maiolino, S.; Pagliara, V.; Ungaro, F.; Tatangelo, F.; Leone, A.; Scalia, G.; Budillon, A.; Quaglia, F.; Russo, G. Enhancement of 5-FU sensitivity by the proapoptotic rpL3 gene in p53 null colon cancer cells through combined polymer nanoparticles. *Oncotarget* **2016**, *7*, 79670−79687.
(32) Kopac, T. Protein corona, understanding the nanoparticle-protein interactions and future perspectives: A critical review. *Int. J. Biol. Macromol.* **2021**, *169*, 290−301.
(33) Miceli, E.; Kar, M.; Calderon, M. Interactions of organic nanoparticles with proteins in physiological conditions. *J. Mater. Chem. B* **2017**, *5*, 4393−4405.
(34) Chen, Q.; Kang, J.; Fu, C. The independence of and associations among apoptosis, autophagy, and necrosis. *Signal Transduction Targeted Ther.* **2018**, *3*, No. 18.
(35) Pecoraro, A.; Pagano, M.; Russo, G.; Russo, A. Ribosome Biogenesis and Cancer: Overview on Ribosomal Proteins. *Int. J. Mol. Sci.* **2021**, *22*, No. 5496.
(36) Pecoraro, A.; Carotenuto, P.; Franco, B.; De Cegli, R.; Russo, G.; Russo, A. Role of uL3 in the Crosstalk between Nucleolar Stress and Autophagy in Colon Cancer Cells. *Int. J. Mol. Sci.* **2020**, *21*, No. 2143.
(37) *Glide*; Schrödinger, LLC: New York, NY, 2021.
(38) Bellavita, R.; Casciaro, B.; Di Maro, S.; Brancaccio, D.; Carotenuto, A.; Falanga, A.; Cappiello, F.; Buommino, E.; Galdiero, S.; Novellino, E.; Grossmann, T. N.; Mangoni, M. L.; Merlino, F.; Grieco, P. First-in-Class Cyclic Temporin L Analogue: Design, Synthesis, and Antimicrobial Assessment. *J. Med. Chem.* **2021**, *64*, 11675−11694.
(39) Merlino, F.; Billard, E.; Yousif, A. M.; Di Maro, S.; Brancaccio, D.; Abate, L.; Carotenuto, A.; Bellavita, R.; d'Emmanuele di Villa Bianca, R.; Santicioli, P.; Marinelli, L.; Novellino, E.; Hebert, T. E.; Lubell, W. D.; Chatenet, D.; Grieco, P. Functional Selectivity Revealed by N-Methylation Scanning of Human Urotensin II and Related Peptides. *J. Med. Chem.* **2019**, *62*, 1455−1467.
(40) Medina-Medina, I.; Martinez-Sanchez, M.; Hernandez-Monge, J.; Fahraeus, R.; Muller, P.; Olivares-Illana, V. p53 promotes its own polyubiquitination by enhancing the HDM2 and HDMX interaction. *Protein Sci.* **2018**, *27*, 976−986.
(41) Daniele, S.; La Pietra, V.; Piccarducci, R.; Pietrobono, D.; Cavallini, C.; D'Amore, V. M.; Cerofolini, L.; Giuntini, S.; Russomanno, P.; Puxeddu, M.; Nalli, M.; Pedrini, M.; Fragai, M.; Luchinat, C.; Novellino, E.; Taliani, S.; Regina, G. L.; Silvestri, R.; Martini, C.; Marinelli, L. CXCR4 antagonism sensitizes cancer cells to novel indole-based MDM2/4 inhibitors in glioblastomabmultiforme. *Eur. J. Pharmacol.* **2021**, *897*, No. 173936.
(42) Merlino, F.; Daniele, S.; Pietra, V. L.; Di Maro, S.; Di Leva, F. S.; Brancaccio, D.; Tomassi, S.; Giuntini, S.; Cerofolini, L.; Fragai, M.; Luchinat, C.; Reichart, F.; Cavallini, C.; Costa, B.; Piccarducci, R.; Taliani, S.; Da Settimo, F.; Martini, C.; Kessler, H.; Novellino, E.; Marinelli, L. Simultaneous Targeting of RGD-Integrins and Dual Murine Double Minute Proteins in Glioblastoma Multiforme. *J. Med. Chem.* **2018**, *61*, 4791−4809.
(43) Espadinha, M.; Lopes, E. A.; Marques, V.; Amaral, J. D.; Dos Santos, D. J. V. A.; Mori, M.; Daniele, S.; Piccarducci, R.; Zappelli, E.; Martini, C.; Rodrigues, C. M. P.; Santos, M. M. M. Discovery of MDM2-p53 and MDM4-p53 protein-protein interactions small molecule dual inhibitors. *Eur. J. Med. Chem.* **2022**, *241*, No. 114637.
(44) *LigPrep*; Schrödinger, LLC: New York, NY, 2021.
(45) *Maestro*; Schrödinger, LLC: New York, NY, 2021.
(46) Banks, J. L.; Beard, H. S.; Cao, Y.; Cho, A. E.; Damm, W.; Farid, R.; Felts, A. K.; Halgren, T. A.; Mainz, D. T.; Maple, J. R.; Murphy, R.; Philipp, D. M.; Repasky, M. P.; Zhang, L. Y.; Berne, B. J.; Friesner, R. A.; Gallicchio, E.; Levy, R. M. Integrated Modeling Program, Applied Chemical Theory (IMPACT). *J. Comput. Chem.* **2005**, *26*, 1752−1780.
(47) *Epik*; Schrödinger, LLC: New York, NY, 2021.
(48) *Prime*; Schrödinger, LLC: New York, NY, 2021.
(49) Bellavita, R.; Falanga, A.; Buommino, E.; Merlino, F.; Casciaro, B.; Cappiello, F.; Mangoni, M. L.; Novellino, E.; Catania, M. R.; Paolillo, R.; Grieco, P.; Galdiero, S. Novel temporin L antimicrobial peptides: promoting self-assembling by lipidic tags to tackle superbugs. *J. Enzyme Inhib. Med. Chem.* **2020**, *35*, 1751−1764.
(50) Cavaco, M.; Valle, J.; Flores, I.; Andreu, D.; Castanho, M. A. Estimating peptide half-life in serum from tunable, sequence-related physicochemical properties. *Clin. Transl. Sci.* **2021**, *14*, 1349−1358.
(51) Virgilio, A.; Benigno, D.; Pecoraro, A.; Russo, A.; Russo, G.; Esposito, V.; Galeone, A. Exploring New Potential Anticancer Activities of the G-Quadruplexes Formed by [(GTG2T(G3T)3] and Its Derivatives with an Abasic Site Replacing Single Thymidine. *Int. J. Mol. Sci.* **2021**, *22*, No. 7040.
(52) Pecoraro, A.; Virgilio, A.; Esposito, V.; Galeone, A.; Russo, G.; Russo, A. uL3Mediated Nucleolar Stress Pathway as a New Mechanism of Action of Antiproliferative G-quadruplex TBA Derivatives in Colon Cancer Cells. *Biomolecules* **2020**, *10*, No. 583.
(53) Virgilio, A.; Esposito, V.; Pecoraro, A.; Russo, A.; Vellecco, V.; Pepe, A.; Bucci, M.; Russo, G.; Galeone, A. Structural properties and anticoagulant/cytotoxic activities of heterochiral enantiomeric thrombin binding aptamer (TBA) derivatives. *Nucleic Acids Res.* **2020**, *48*, 12556−12565.
(54) Schmittgen, T. D.; Livak, K. J. Analyzing real-time PCR data by the comparative C(T) method. *Nat. Protoc.* **2008**, *3*, 1101−1108.
(55) Russo, A.; Russo, G.; Cuccurese, M.; Garbi, C.; Pietropaolo, C. The 3′-untranslated region directs ribosomal protein-encoding mRNAs

to specific cytoplasmic regions. *Biochim. Biophys. Acta, Mol. Cell Res.* **2006**, *1763*, 833−843.
(56) Mosca, L.; Pagano, M.; Pecoraro, A.; Borzacchiello, L.; Mele, L.; Cacciapuoti, G.; Porcelli, M.; Russo, G.; Russo, A. S-Adenosyl-l-Methionine Overcomes uL3-Mediated Drug Resistance in p53 Deleted Colon Cancer Cells. *Int. J. Mol. Sci.* **2021**, *22*, No. 103.

https://doi.org/10.1021/acs.jmedchem.3c01312
J. Med. Chem. 2024, 67, 1812−1824